

李会来, 李凡, 张鼎文, 等. 低温剥蚀 LA-ICP-MS 准确测定硫化物矿物多元素分析研究 [J]. 岩矿测试, 2023, 42(5): 970–982. doi: 10.15898/j.ykcs.202308290144.

LI Huilai, LI Fan, ZHANG Dingwen, et al. Multi-element Accurate Analysis of Sulfide Minerals by Low-temperature Ablation LA-ICP-MS [J]. Rock and Mineral Analysis, 2023, 42(5): 970–982. doi: 10.15898/j.ykcs.202308290144.

## 低温剥蚀 LA-ICP-MS 准确测定硫化物矿物多元素分析研究

李会来, 李凡, 张鼎文, 郭伟, 靳兰兰, 胡圣虹\*

(中国地质大学(武汉)生物地质与环境地质国家重点实验室, 中国地质大学(武汉)地球科学学院, 湖北 武汉 430074)

**摘要:** 硫化物矿物中元素含量及其分布可示踪硫化物成矿过程、辨别金属来源和沉积过程的物理化学条件, 在地质学、矿床学等领域具有重要的应用价值。激光剥蚀电感耦合等离子体质谱(LA-ICP-MS)已成功应用于硫化物矿物元素微区分析研究, 但激光与物质作用产生的热效应严重制约分析结果的可靠性。本文建立了一种高精密度、高准确度的低温剥蚀 LA-ICP-MS 测定硫化物矿物多元素方法。采用自行研制的 Peltier 低温剥蚀池可有效抑制硫化物矿物 LA-ICP-MS 分析中的热效应, 提高分析结果的精密度和准确度。扫描电子显微镜(SEM)表明: 在低温( $-30^{\circ}\text{C}$ )条件下可在一定程度地抑制激光剥蚀引起的热效应, 减少样品熔化和气溶胶气相再沉积; 而通过气溶胶颗粒分析发现低温剥蚀可以减小样品气溶胶颗粒的平均尺寸, 得到的颗粒粒径分布范围也较小。不同元素信号强度的精密度(RSD)从常温下的 20.1%~34.4% 改善到 11.5%~15.8%, 元素的检出限为  $0.054\sim0.077\mu\text{g/g}$ 。将该低温 LA-ICP-MS 系统应用于实验室内部标样黄铜矿 Ccp-1 分析, 测定值与参考值之间的标准偏差在 7% 以内。

**关键词:** 低温剥蚀池; 硫化物矿物; 激光剥蚀行为; 热效应; LA-ICP-MS

### 要点:

- (1) 采用研制的低温剥蚀池, 改善了激光与物质的作用效率, 建立了低温剥蚀 LA-ICP-MS 准确测定硫化物矿物多元素微区分析方法。
- (2) 采用低温( $-30^{\circ}\text{C}$ )剥蚀池, 抑制了硫化物矿物激光剥蚀过程中的热效应, 局部热熔区和气相再沉积区明显减小。
- (3) 激光剥蚀气溶胶粒径实验表明, 低温条件下产生的气溶胶颗粒粒径和团聚体明显较小, 提高了气溶胶的传输和电离效率。

**中图分类号:** O657.63; P578.2

**文献标识码:** A

硫化物矿物的微区元素、同位素地球化学信息在研究硫化物矿物的形成机制和演化过程起着至关重要的作用, 如 Co、Ni 的含量可用来判别黄铁矿的形成环境; Pb 同位素组成反映了硫化物矿物形成时原始热液的初始 Pb 同位素特征, 可作为研究成矿时代和物质来源的示踪剂; 闪锌矿中 Fe、Mn、Ge 等元素含量也常用于确定成矿温度等<sup>[1-7]</sup>。激光剥蚀电

感耦合等离子体(LA-ICP-MS)微区原位分析技术已被广泛应用于硫化物矿物元素浓度、同位素组成的研究, 取得了大量创新性成果<sup>[8-12]</sup>。由于硫化物矿物独特的物理和化学性质, 其激光剥蚀行为往往有别于其他样品(如硅酸盐熔融玻璃)。最直观的现象是激光热效应导致剥蚀坑附近产生熔化和硫化物气溶胶气相再沉积, 在剥蚀坑周围呈现大量的样品颗

收稿日期: 2023-08-14; 修回日期: 2023-09-06; 接受日期: 2023-09-16

基金项目: 国家重点研发计划项目(2021YFC2903000)课题“战略性矿产微区原位分析技术及应用”

第一作者: 李会来, 博士研究生, 地球化学专业。E-mail: 191455426@qq.com。

通信作者: 胡圣虹, 教授, 博士生导师, 主要从事分析化学、分析地球化学的教学与研究工作。E-mail: shhu@cug.edu.cn。

粒沉积, 这是限制硫化物矿物样品分析精密度和准确性的主要因素<sup>[13-15]</sup>。

早在 20 世纪 90 年代, Watling 等<sup>[13]</sup>研究证实, 由于红外激光与物质作用时产生强烈热效应会导致严重的热融蚀和大颗粒气溶胶再沉积, 采用红外激光(1064nm Nd:YAG 激光)直接定量硫化物矿物中的元素含量是不可能的。后续研究采用四倍频、五倍频的 266nm 和 213nm 的紫外波长激光, 通过降低热效应和气溶胶粒径来提高元素的分析精密度, 但获得的分析精密度仍然较差<sup>[16-17]</sup>。Hergenröder 等<sup>[18]</sup>系统研究了不同波长的纳秒激光与物质的相互作用产生的气溶胶行为, 证实长波长(红外和紫外)激光形成的剥蚀坑形状不规则、热附带损伤大、热效应造成的熔融层较多、表面沉积的样品颗粒较多。Guillong 等<sup>[19]</sup>对比研究了 266nm、213nm 和 193nm 激光剥蚀行为, 发现 193nm 激光剥蚀时气溶胶粒径更细, 热效应更弱, 各元素的 RSD 均小于 20%。换句话说, 采用波长较短的深紫外激光剥蚀系统(如 157nm、193nm), 光子和物质之间的碰撞会加剧<sup>[20-21]</sup>, 有助于减少熔化区和气溶胶颗粒的大小, 提高元素、同位素分析的准确度和精密度。然而, 在深紫外的 193nm 激光剥蚀过程中仍然存在一定程度的热效应, 尤其是剥蚀硫化物矿物类样品。Fernández 等<sup>[22]</sup>发现采用 193nm 激光剥蚀过程中仍存在一定的熔化层, 导致大颗粒气溶胶的形成。柯于球等<sup>[23]</sup>利用 193nm ArF 准分子激光研究了熔融温度对硫化矿物激光剥蚀形貌和元素分馏效应的影响。Kuhn 等<sup>[24]</sup>研究了激光剥蚀黄铜矿的粒度和形貌, 指出不可控的剥蚀过程可能导致测定结果不准确。研究人员提出了不同的方法来改善硫化物激光剥蚀过程中的热效应。Mueller 等<sup>[25]</sup>发现, 与点剥蚀相比, 线扫描的精密度可提高 50%。Guillong 等<sup>[26]</sup>的研究结果表明, 在载气中加入少量的氢可以将测试的 47 种元素的灵敏度提高 2 倍至 4 倍。采用更短的脉冲宽度飞秒激光可改善硫化物矿物激光剥蚀微区分析的热效应<sup>[27-31]</sup>。尽管如此, 深紫外波长和短脉冲宽度的激光在剥蚀过程中还是存在一定的局部热效应, 如何抑制剥蚀过程中的热效应获取可靠的分析结果, 仍然是硫化物矿物元素微区分析中的难点。改善激光与物质作用的环境, 采用低温剥蚀池有可能抑制激光剥蚀硫化物矿物时产生的局部热效应。近年来, 有关低温剥蚀池的研究为冰芯、植物、血液及生物软组织等样品的 LA-ICP-MS 分析提供了可能。Reinhardt 等<sup>[32]</sup>率先设计了一款低温剥蚀池(冷却

液为硅油), 其可调温度下限为-45℃, 采用 LA-ICP-MS 成功地分析了极地冰芯中的元素分布, 极低的温度保证冰芯样品内部元素不发生改变, 有效地防止了样品原始信息失真。Feldmann 等<sup>[33]</sup>设计了一个内体积约为 60cm<sup>3</sup> 的液氮制冷式圆型低温剥蚀池应用于生物软组织的分析, 该低温剥蚀池的温度范围为-20℃ 至-100℃, 但控温精度较差。Wang 等<sup>[34]</sup>自制的一款半导体制冷低温剥蚀池具有温控精准和换样方便的优势, 用于香菜叶片的 LA-ICP-MS 微区分析, 结果表明在低温剥蚀环境下可以得到规整的剥蚀坑, 有效地提高了微区成像的空间分辨率。本课题组采用自行研制的低温剥蚀池<sup>[35-36]</sup>与 LA-ICP-MS 结合成功用于血液和脑脊液等临床样品中微量元素高通量分析。因此, 采用低温剥蚀池可能是解决硫化物矿物这类具有特定的物理化学性质样品微区多元素的准确分析、抑制激光剥蚀过程中热效应的一种新途径。

本研究采用研制的小体积低温剥蚀池, 结合 LA-ICP-MS 用于硫化物矿物多元素同时检测, 探讨低温剥蚀池对于激光剥蚀行为的改善效果, 观察不同温度样品在 LA-ICP-MS 分析过程中存在的热熔体区以及剥蚀颗粒再沉积现象, 分析激光剥蚀过程热效应对于元素信号精密度和准确度的影响。

## 1 实验部分

### 1.1 仪器及工作参数

实验使用的 LA-ICP-MS 系统为 GeoLas HD 193nm ArF 准分子激光剥蚀系统(德国 Coherent 公司)与 7700x 电感耦合等离子体质谱仪(美国 Agilent 公司)。表 1 所示为 LA-ICP-MS 工作参数。在实验参数优化前, LA-ICP-MS 系统预热约 30min。氦气作为载气、氩气作为补偿气将激光剥蚀的气溶胶从剥蚀池输送到 ICP-MS。采用 NIST SRM610 玻璃标准进行仪器参数优化, 确保不同质量数元素<sup>7</sup>Li、<sup>89</sup>Y 和<sup>238</sup>U 获得最大信号强度和最佳精密度, 同时保持 ThO/Th 比值<0.3% 和 U/Th 比值接近 1。

SU8010 型高分辨率场发射扫描电镜(日本 Hitachi 公司)用于剥蚀坑和剥蚀气溶胶的形貌分析, Nano-ZS90 型纳米激光粒度仪(英国 Malvern 公司)用于表征气溶胶的颗粒尺寸和分布。

### 1.2 实验样品和主要试剂

NIST SRM610 标准参考融熔玻璃样品、MASS-1 混合冷压硫化物标准物质(美国国家标准与技术研究院)用于本实验研究。

表1 LA-ICP-MS 仪器工作参数

Table 1 The operating conditions of LA-ICP-MS.

电感耦合等离子体质谱 ICP-MS(7700x)		激光剥蚀系统 Laser system(GeoLas HD)	
参数	工作条件	参数	工作条件
RF 功率	1550W	激光波长	193nm
反馈功率	8W	能量密度	6J/cm <sup>2</sup>
RF 电压	1.60W	剥蚀斑径	60μm
采样深度	7.5mm	激光频率	5Hz
载气(Ar)流速	0.85L/min	剥蚀气(He)流速	0.4L/min
元素	<sup>55</sup> Mn, <sup>57</sup> Fe, <sup>59</sup> Co, <sup>60</sup> Ni, <sup>63</sup> Cu, <sup>66</sup> Zn, <sup>71</sup> Ga, <sup>74</sup> Ge, <sup>75</sup> As, <sup>111</sup> Cd, <sup>208</sup> Pb		

实验室自制含多元素硫化物矿物参考样品。采用文献介绍的水热法<sup>[37]</sup>合成了黄铜矿和黄铁矿硫化物纳米颗粒,加入单元素标准溶液并混合,将所得混合物干燥、研磨、粉碎、填胶、抛光,制成含有多种元素的实验室内部固体参考物质(Ccp-1 和 Py-1),浓度范围为1~20μg/g。

9个硫化物矿物实际样品包括黄铁矿1-3、方铅矿1-3和闪锌矿1-3,切割成边长为2cm,厚度约为8mm的块状,然后抛光成镜面状用于实际样品分析检测。

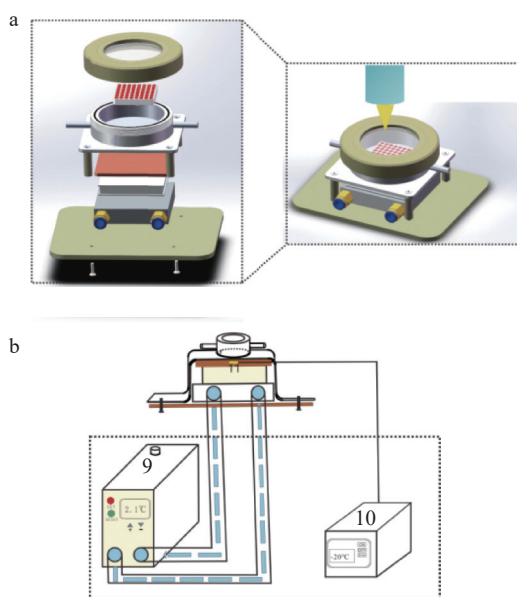
超纯水(电阻率18.2MΩ·cm)采用Milli-Q净水系统(美国Millipore公司)制得。

### 1.3 低温剥蚀池结构

本研究采用了本课题组研制的低温剥蚀池<sup>[35]</sup>(图1)。低温剥蚀池的材料为铝合金,具有良好的导热性。剥蚀池内部体积约为12.56cm<sup>3</sup>,进、出口直径分别为1mm和4mm。较小的入口和较大的出口增加了气溶胶从剥蚀池中被更快速传输的效率,从而提高了进入等离子体的瞬时气溶胶颗粒浓度。由Peltier元件冷却的铜板贴在剥蚀池单元的底部用以散热,位于Peltier元件下方是内部热交换的水冷平台,冷却水被泵入其中以提取产生的热量。外部冷水机包括一组Peltier元件和确保冷却水再冷却以及再循环的电机。温度控制装置通过导线连接到Peltier元件上,可以调节剥蚀池的温度。将温度探头插入铜板以监测剥蚀池的温度。

### 1.4 激光气溶胶颗粒收集实验

为研究不同温度条件下硫化物矿物激光剥蚀时产生的气溶胶颗粒尺寸及分布,在剥蚀池的出口处安装了0.1μm孔径的滤膜用于收集剥蚀后的气溶胶颗粒。分别在室温(20℃)和低温(-30℃)下,在表1所示工作条件下连续剥蚀硫化物标准物质MASS-1约2min,用滤膜上收集气溶胶颗粒并进行扫描电镜分析。



a. 低温剥蚀池的内部结构(1—剥蚀池; 2—氟化钙窗口; 3—PEEK盖; 4—导热铜板; 5—Peltier元件; 6—水冷平台; 7—底板; 8—载物台); b. 剥蚀池的外部制冷系统(9—循环制冷机; 10—温控系统; 11—测温元件)。

a. Interior structure of the cryogenic ablation cell (1—Ablation cell; 2—Calcium fluoride window; 3—PEEK lid; 4—Thermally conductive copper plate; 5—Peltier element; 6—Water-cooled platform; 7—Baseplate; 8—Stage); b. Ablation cell with the external refrigeration system (9—Cycle refrigeration machine; 10—Temperature control device; 11—Temperature sensor).

图1 低温剥蚀池结构示意图

Fig. 1 Schematic diagram of the low-temperature ablation cell structure.

为进一步比较低温和室温条件下激光剥蚀产生的气溶胶颗粒的尺寸分布,使用超纯水在上述相同的仪器条件下收集气溶胶,采用Nano-ZS90纳米激光粒度仪(英国Malvern公司)测量其气溶胶颗粒尺寸和分布。

### 1.5 分析步骤

在本研究中,采用MASS-1作为外部校正标准,

选择S作为内部校正标准对硫化物进行定量分析。硫化物样品在低温( $-30^{\circ}\text{C}$ )剥蚀池中预先冷冻约5min,然后进行LA-ICP-MS样品采集与分析。在数据采集之前,激光束聚焦在矿物表面,激光剥蚀样品产生的气溶胶由载气输送到ICP-MS中。所有硫化物样品均采用点剥蚀模式进行三次重复分析,每次分析过程包括载气的10s背景信号和60s数据采集,且在两次剥蚀之间设置了10s的清洗时间,以尽量减少或防止记忆影响。为校正分析过程中可能的仪器分析信号漂移,以10个样品为间隔分析外部校正标准。

## 2 结果与讨论

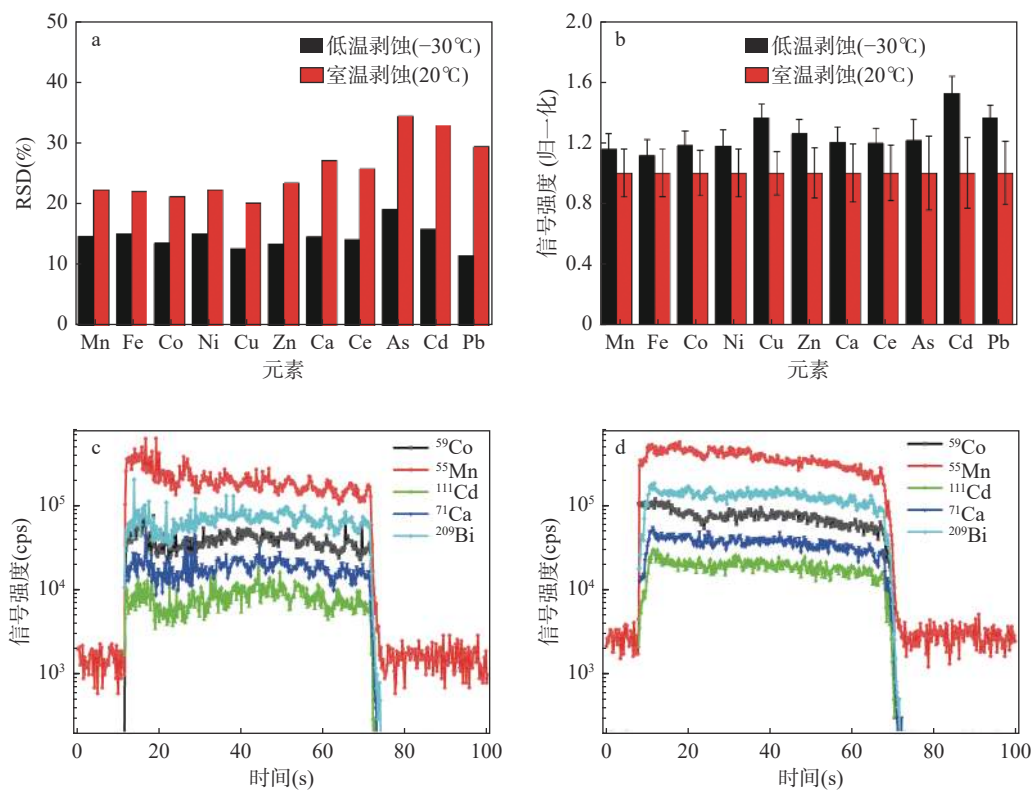
### 2.1 剥蚀池温度对分析信号强度和精密度的影响

利用自行研制的剥蚀池,在低温( $-30^{\circ}\text{C}$ )和室温( $20^{\circ}\text{C}$ )条件下,采用点剥蚀模式对MASS-1标样进行分析,对比两种温度下元素信号强度和精密度变化。在室温下,元素信号的RSD范围为 $20.1\% \sim 34.4\%$ ,低温剥蚀样品时元素信号的RSD均小于15.8%

(图2a)。不同元素的信号强度提高了11%至52%(图2b)。图2c为MASS-1样品在室温下的时间信号分辨谱图,可以观察到明显的波动和尖峰,而低温下的时间分辨信号表现出较好的稳定性,元素信号的波动远小于室温下元素信号的变化(图2d)。Jarošová等<sup>[38]</sup>研究了激光剥蚀铅样品时样品温度对于分馏的影响,发现在干冰温度下各元素信号精密度有一定改善,这可能是低温可以更好地传递剥蚀点处的热能。结合本实验结果表明,随着剥蚀温度降低,各元素的分析灵敏度会不同程度的提高,分析信号的RSD明显降低。这是由于低温剥蚀环境在一定程度上改善了硫化物矿物激光剥蚀行为,抑制了激光与物质作用的热效应,减少了样品中局部热能的积累和热效应引起的熔体区。

### 2.2 剥蚀池温度对硫化物矿物激光剥蚀行为的影响

为探讨不同剥蚀池温度下硫化物矿物激光剥蚀行为的影响,实验选择激光剥蚀斑径为 $60\mu\text{m}$ ,能量密度为 $8\text{J/cm}^2$ ,剥蚀频率为5Hz,以点剥蚀方式剥蚀



a—分析信号精密度; b—分析信号强度(以室温剥蚀下元素信号强度做归一化),  $n=3$ ; c—室温下元素的时间信号分辨谱图; d—低温下元素的时间信号分辨谱图。

a—Analytical signal precision; b—Analytical signal intensity (Normalization is based on element signal intensity at room temperature),  $n=3$ ; c—Time signal resolution spectrum of elements at room temperature; d—Time signal resolution spectrum of elements at low temperature.

图2 MASS-1 在不同剥蚀温度下的剥蚀信号对比情况

Fig. 2 Comparison of signals of MASS-1 at different ablation temperatures.

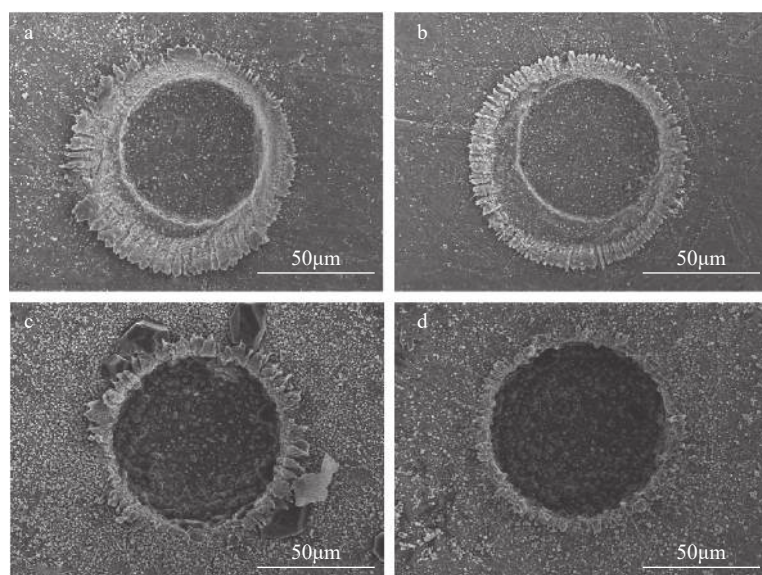
实验室固体矿物黄铜矿 Ccp-1 和黄铁矿 Py-1, 利用扫描电镜(SEM)观察在不同温度条件下的剥蚀坑形貌变化。如图 3a 所示常温下黄铜矿 Ccp-1 上的剥蚀坑呈两层环状结构, 其中内层为浅色熔融带, 外层为白色气溶胶气相沉积物, 而低温下熔体层更少, 颗粒沉积带更薄(图 3b); 图 3 中 c 和 d 所示常温下黄铁矿 Py-1 剥蚀坑周围的熔融带比低温下熔融带更为明显, 更多的非剥蚀区域的样品在室温下被熔融。室温下两种硫化物矿物剥蚀坑周围大量的熔融喷射物表明在室温下形成的剥蚀坑均比在低温下形成的剥蚀坑显示出更严重的热熔融现象, 相比之下, 低温下剥蚀坑没有明显的热熔融现象, 且其底部更平坦, 大的熔融球形颗粒数量减少。说明降低温度可以改善硫化矿物的激光剥蚀过程。而柯于球等<sup>[23]</sup> 观察了不同硫化物矿物表现出的剥蚀坑形貌, 推测剥蚀晕的大小和形状差异可能与不同硫化物矿物的熔点有关。低温剥蚀池的使用抑制了激光与物质作用的热效应, 减弱了硫化物矿物表面的熔融现象, 从而产生更小的气溶胶颗粒, 进一步提高了气溶胶的传输和电离效率。

### 2.3 剥蚀池温度对硫化物矿物剥蚀气溶胶粒径的影响

为进一步考察了不同温度下硫化物矿物激光剥蚀气溶胶颗粒的粒径大小和分布情况。设计了激光剥蚀气溶胶颗粒收集实验, 在剥蚀池的传输出品采

用孔径为  $0.1\mu\text{m}$  的滤膜进行不同剥蚀池温度气溶胶的收集, 利用扫描电镜(SEM)对所采集的颗粒的形状和大小进行了分析。分别在室温和低温下, 以  $6\text{J}/\text{cm}^2$  的能量密度连续剥蚀硫化物标准物质 MASS-1 约 2min。图 4 所示的 SEM 图像表明, 室温下产生的颗粒较大, 形成了较大的团聚体(图 4a), 而在低温  $-30^\circ\text{C}$  下产生的颗粒较小, 团聚体较少(图 4c)。这种室温下的团聚体的形状和细丝连接表明颗粒形成过程中存在强电荷<sup>[39-40]</sup>。此外, 在室温比低温下产生的气溶胶中大颗粒气溶胶明显增多(图 4 中 b, d), 这些颗粒大小和形状的差异反映了剥蚀过程中发生的熔化和熔体喷射过程的不同。

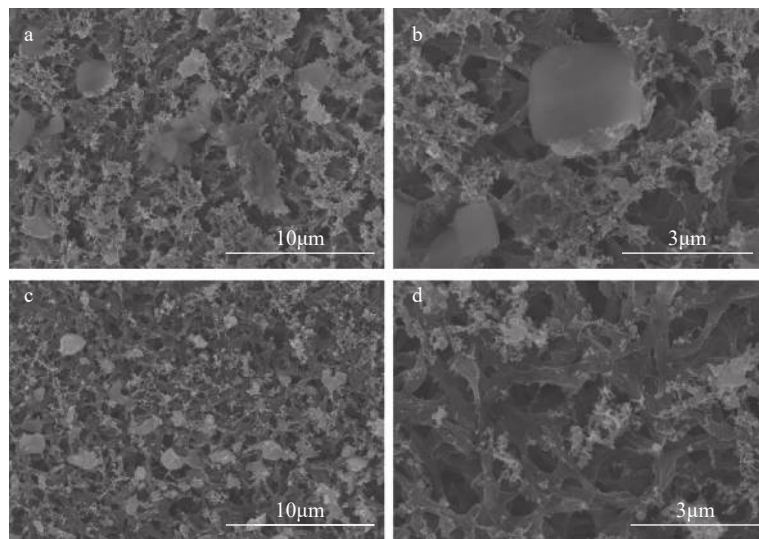
图 5 所示为采用激光粒度仪测定的不同剥蚀池温度条件下激光剥蚀气溶胶粒径分布图。从图中可以看出, 室温下气溶胶粒径分布呈现双峰型, 主要集中在  $300\text{nm}$  和  $700\text{nm}$  处。同样的, 在  $-30^\circ\text{C}$  时的粒径分布也呈现双峰型, 但其直径波峰约为  $190\text{nm}$  和  $400\text{nm}$ , 平均颗粒粒径小于室温条件且气溶胶尺寸分布范围更小。低温条件下产生的细颗粒气溶胶可以改善 ICP 中气溶胶的传输和电离效率, 减少元素分馏, 增强信号强度和稳定性, 从而提高 ICP-MS 的分析性能。值得注意的是, 这一实验研究是定性的比较在不同温度下产生的气溶胶颗粒变化, 而不是定量地确定其大小和分布。



a— $20^\circ\text{C}$  的黄铜矿; b— $-30^\circ\text{C}$  的黄铜矿; c— $20^\circ\text{C}$  的黄铁矿; d— $-30^\circ\text{C}$  的黄铁矿。剥蚀条件: 激光能量密度  $8\text{J}/\text{cm}^2$ , 剥蚀斑径为  $60\mu\text{m}$ 。  
a—Chalcopyrite at  $20^\circ\text{C}$ ; b—Chalcopyrite at  $-30^\circ\text{C}$ ; c—Pyrite at  $20^\circ\text{C}$ ; d—Pyrite at  $-30^\circ\text{C}$ . Ablation conditions: laser energy density is  $8\text{J}/\text{cm}^2$ . Spot diameter is  $60\mu\text{m}$ .

图3 硫化物矿物在不同剥蚀温度下剥蚀形貌的扫描电子显微镜图

Fig. 3 Scanning electron microscopy maps of sulfide minerals morphology at different ablation temperatures.

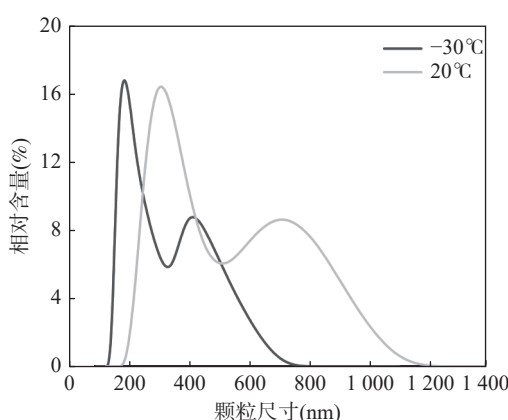


a—常温 20℃ 下激光剥蚀颗粒, 放大倍率 5000×; b—常温 20℃ 下激光剥蚀颗粒, 放大倍率 15000×; c—低温-30℃ 下激光剥蚀颗粒, 放大倍率 5000×; d—低温-30℃ 下激光剥蚀颗粒, 放大倍率 15000×。剥蚀条件: 激光能量密度为  $6\text{J}/\text{cm}^2$ , 连续剥蚀 2min。

a—Laser particles at 20℃ with 5000× magnification; b—Laser particles at 20℃ with 15000× magnification; c—Laser particles at -30℃ with 5000× magnification; d—Laser particles at -30℃ with 15000× magnification. Ablation conditions: laser energy density is  $6\text{J}/\text{cm}^2$ , continuous ablation for 2min.

图4 收集 MASS-1 在不同温度下激光剥蚀后气溶胶颗粒的扫描电子显微镜图

Fig. 4 Scanning electron microscope maps of aerosol particles after MASS-1 ablated at different temperatures.



剥蚀条件: 激光能量密度为  $6\text{J}/\text{cm}^2$ , 连续剥蚀 2min。

Ablation conditions: laser energy density is  $6\text{J}/\text{cm}^2$ , continuous ablation for 2min.

图5 收集 MASS-1 在不同温度下激光剥蚀后气溶胶颗粒的粒径分布图

Fig. 5 Particle size distribution of aerosol particles after MASS-1 ablated at different temperatures.

#### 2.4 剥蚀池温度对激光工作参数的影响

LA-ICP-MS 分析的精密度受多种仪器参数的影响, 其中最重要的是能量密度和剥蚀斑径。为了研究样品温度是否也会影响不同能量密度和光斑直径下的剥蚀行为, 将混合硫化物标准样品 MASS-1 在低温和室温条件下进行剥蚀。Co 信号作为信号稳

定性指标进行监测。如图 6 所示, 无论能量密度如何变化, 信号在低温时稳定性较好, 增加到  $6\text{J}/\text{cm}^2$  时趋于稳定。同样, 斑径直径与能量密度变化趋势一致,  $60\mu\text{m}$  斑径获得最好的精密度。上述结果表明, 在不同的仪器工作条件下, 采用低温剥蚀池都可以明显地改善硫化物矿物 LA-ICP-MS 分析的准确度和精密度。

### 3 分析性能

#### 3.1 方法检出限

依据 Longrich 等<sup>[4]</sup> 定义检出限为载气(气体空白)信号的 3 倍标准偏差计算, Mn、Co、Ni、Ga、Ge、As 和 Cd 元素的检出限分别为 0.068、0.054、0.063、0.061、0.057、0.077 和  $0.059\mu\text{g/g}$ 。

#### 3.2 方法准确度和精密度

以标准物质 MASS-1 为外标, S 元素为内标。对实验室自制的硫化物内部标准黄铜矿 Ccp-1 中常用的几种微量元素(Mn、Co、Ni、Ga、Ge、As、Cd)在低温下( $-30^\circ\text{C}$ )进行了测定。结果通过时间信号分辨谱图采集得到, 信号采集时间为 60s, 斑径直径为  $60\mu\text{m}$ , 激光频率为 5Hz。如表 2 所示, 所有元素的测试值与参考值之间的标准偏差在 7% 以内, RSD 范围为 7% ~ 12%。

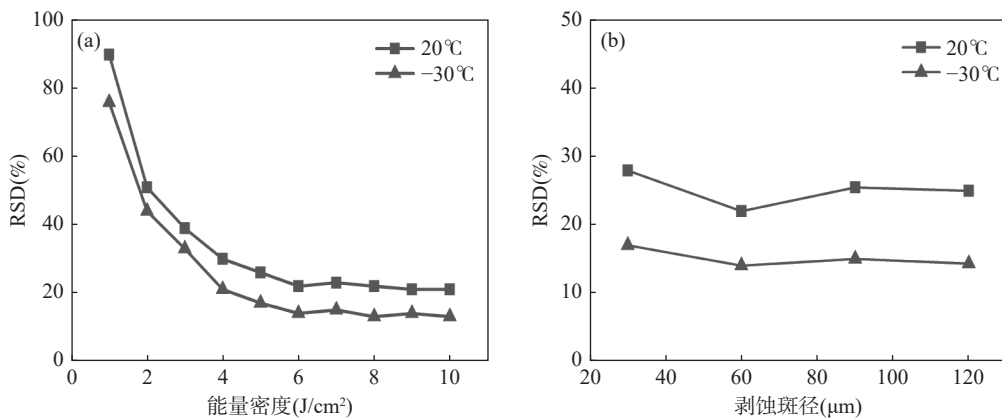


图6 低温剥蚀池在不同激光条件下(a)能量密度和(b)剥蚀斑径的性能对比(样品为MASS-1)

Fig. 6 Performance comparison of the low-temperature ablation cell under different laser conditions: (a) energy density and (b) ablation diameter (The sample is MASS-1).

## 4 实际样品分析

### 4.1 不同分析温度的比较

如上所述分析方法,采用实验室自制的校准标准品黄铜矿Ccp-1分别在低温和室温进行分析,对比不同分析温度下的分析结果。如表2所示,Mn、Ge、As、Cd等元素在室温下的测定值均低于标准参考值10%以上,分析精密度较差;而在低温条件下的测定值与参考值吻合较好,分析精密度显著提高。这是由于该方法可以改善激光剥蚀行为,产生更多的细颗粒气溶胶。

### 4.2 硫化物矿物实际样品测试

表3所示为硫化物矿物实际样品的结果。采用所建立的方法测定每个样品中Mn、Co、Ni、Ga、Ge、As和Cd的浓度,并计算三次测量的平均值和标准差,测定结果与溶液ICP-MS法基本一致。证实本方法精密度高,适用于硫化物样品中多元素的分析。

## 5 结论

基于自行研制的低温剥蚀池,建立了一种高精度高准确度测定硫化物矿物中多元素的低温剥蚀LA-ICP-MS分析方法。该方法有效地抑制了剥蚀过程中的热效应,改善了激光剥蚀行为,减小了气溶胶颗粒尺寸,提高了分析信号的精密度和灵敏度。与常温(20℃)相比,在低温(-30℃)下的元素信号精密

表2 黄铜矿Ccp-1中多元素分析结果( $n=3$ )Table 2 The results of elemental analysis in Ccp-1 ( $n=3$ ).

元素	参考值 ( $\mu\text{g/g}$ )	测定值(-30℃) ( $\mu\text{g/g}$ )	测定值(20℃) ( $\mu\text{g/g}$ )
Mn	7.35±0.43	7.23±0.55	6.15±0.92
Co	5.30±0.36	5.15±0.36	4.76±0.66
Ni	7.75±0.64	7.44±0.53	6.64±0.96
Ga	8.20±0.56	8.34±0.63	7.31±1.25
Ge	8.53±1.29	8.47±0.66	6.82±1.37
As	16.51±1.19	16.96±1.32	13.47±2.56
Cd	0.24±0.01	0.26±0.03	0.21±0.05

度(RSD)明显改善,RSD从常温下的20.1%~34.4%提高到11.5%~15.8%;而相较于常温,低温下元素信号灵敏度提高了11%~52%;元素的检出限为0.054~0.077 $\mu\text{g/g}$ 。所建立方法用于实验室内部标样黄铜矿Ccp-1分析,测定值与参考值之间具有很好的一致性,相对偏差在7%以内。

不同类型的天然硫化物矿物具有不同的热导系数,该方法对各类硫化物矿物带来的改善也不完全相同。而低温会导致气溶胶黏度的增加,后期工作将也深入研究不同温度条件对各类硫化物矿物颗粒分析结果的影响,并验证是否可以通过降低温度来提高长脉宽(ns)激光器的分析性能,使其与短脉宽(fs)激光器的性能相匹配。

表 3 硫化物矿物的元素分析结果( $n=3$ )Table 3 The analytical results of elements in sulfide samples ( $n=3$ )

元素	黄铁矿-1			黄铁矿-2			黄铁矿-3		
	测定值 ( $\mu\text{g/g}$ )	SD ( $\mu\text{g/g}$ )	参考值 ( $\mu\text{g/g}$ )	测定值 ( $\mu\text{g/g}$ )	SD ( $\mu\text{g/g}$ )	参考值* ( $\mu\text{g/g}$ )	测定值 ( $\mu\text{g/g}$ )	SD ( $\mu\text{g/g}$ )	参考值* ( $\mu\text{g/g}$ )
Mn	2.62	0.03	2.68	12.85	1.38	13.58	23.98	0.65	24.69
Co	42.04	2.53	43.76	50.07	5.91	53.1	57.25	2.68	59.33
Ni	247.2	12.11	256.36	256.04	37.01	273.86	257.58	10.29	266.36
Ga	2.95	0.18	2.89	15.76	1.23	14.66	29.61	1.44	28.72
Ge	48.05	4.65	47.25	45.97	23.14	39.04	42.03	2.5	41.04
As	13	1.92	11.26	24.77	3.36	23.49	36.52	5.72	35.01
Cd	0.09	0.01	0.09	0.55	0.03	0.56	1.05	0.09	1.07
元素	方铅矿-1			方铅矿-2			方铅矿-3		
	测定值 ( $\mu\text{g/g}$ )	SD ( $\mu\text{g/g}$ )	参考值* ( $\mu\text{g/g}$ )	测定值 ( $\mu\text{g/g}$ )	SD ( $\mu\text{g/g}$ )	参考值* ( $\mu\text{g/g}$ )	测定值 ( $\mu\text{g/g}$ )	SD ( $\mu\text{g/g}$ )	参考值* ( $\mu\text{g/g}$ )
Mn	0.47	0.06	0.5	3.52	0.53	3.77	7.1	0.53	7.42
Co	0.37	0.05	0.41	2.7	0.21	2.82	5.58	0.26	5.78
Ni	0.52	0.06	0.55	3.29	0.52	3.72	7.89	0.84	10.92
Ga	0.64	0.06	0.63	4.93	0.35	5.15	10.59	0.53	10.81
Ge	0.57	0.06	0.48	4.39	0.12	3.62	9.65	0.47	7.33
As	0.48	0.03	0.42	3.9	0.58	3.54	7.34	0.47	8.69
Cd	0.04	0.01	0.04	0.24	0.04	0.24	0.48	0.09	0.49
元素	闪锌矿-1			闪锌矿-2			闪锌矿-3		
	测定值 ( $\mu\text{g/g}$ )	SD ( $\mu\text{g/g}$ )	参考值* ( $\mu\text{g/g}$ )	测定值 ( $\mu\text{g/g}$ )	SD ( $\mu\text{g/g}$ )	参考值* ( $\mu\text{g/g}$ )	测定值 ( $\mu\text{g/g}$ )	SD ( $\mu\text{g/g}$ )	参考值* ( $\mu\text{g/g}$ )
Mn	2.86	0.42	3.2	12.41	0.56	12.85	25.14	3.76	26.93
Co	0.93	0.03	0.96	8.64	0.47	8.98	17.49	1.73	18.44
Ni	18.75	2.93	20.23	9.89	0.88	10.36	21.08	8.61	24.44
Ga	1.46	0.18	1.49	14.19	0.53	14.48	28.49	2.23	28.31
Ge	0.84	0.11	0.96	10.03	1.36	10.3	18.49	0.74	17.96
As	4.91	0.67	5.01	16.45	2.15	16.79	28.54	3.96	29.12
Cd	1.82	0.18	1.86	2.09	0.09	2.13	2.47	0.35	2.52

注: “\*”表示硫化物实际样品的元素浓度参考值由 ICP-MS 测试得到。

## Multi-element Accurate Analysis of Sulfide Minerals by Low-temperature Ablation LA-ICP-MS

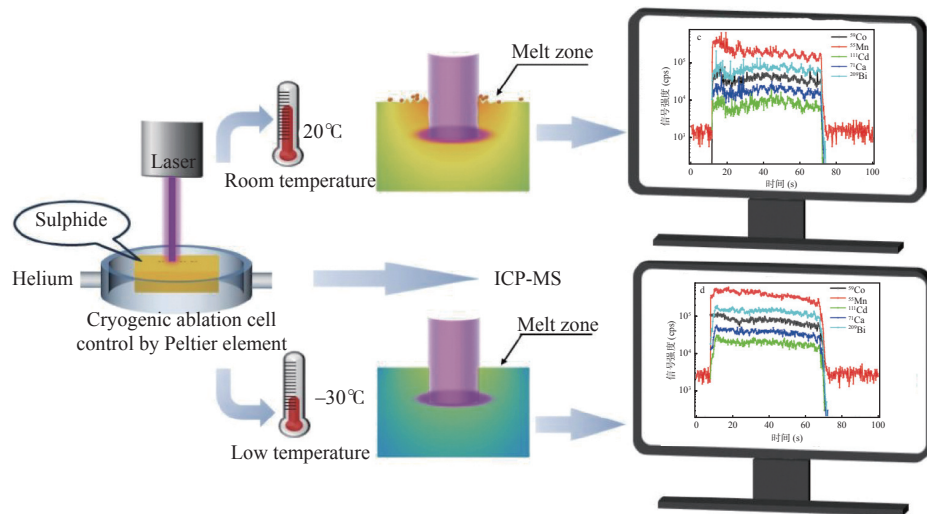
LI Huilai, LI Fan, ZHANG Dingwen, GUO Wei, JIN Lanlan, HU Shenghong\*

(State Key Laboratory of Biogeology and Environmental Geology, College of Earth Sciences, China University of Geosciences (Wuhan), Wuhan 430074, China)

### HIGHLIGHTS

- The developed low temperature ablation cell improved the action efficiency of laser and material, and the high precision and high accuracy multi-elements analytical method in sulfide mineral by LA-ICP-MS were established.
- The low temperature ablation cell ( $-30^{\circ}\text{C}$ ) was used to inhibit the thermal effect of the sulfide mineral laser ablation process, and the local thermal melting area and gas redeposition area were significantly reduced.
- The particle size experiment of laser ablation aerosol shows that the particle size and aggregate of aerosol

produced at low temperature are obviously small, which improves the transport and ionization efficiency of the aerosol.



## ABSTRACT

**BACKGROUND:** Micro-geochemical information of sulfide minerals plays a crucial role in the field of geochemistry, allowing discovery of the formation mechanism and evolution process of sulfide minerals by analyzing their element composition characteristics. LA-ICP-MS is currently the most popular microanalysis technology used for sulfide analysis, having yielded successful results. Due to their unique physical and chemical properties, sulfide mineral samples show different laser ablation behavior to conventional geological samples. The most intuitive phenomenon is the melting of ablation carters caused by laser thermal effect and the deposition of a large number of material particles around the ablation carters, which is the main factor limiting the precision and accuracy of sulfide sample analysis.

Walting et al<sup>[13]</sup> found that direct quantitation of multi-elements in sulfide minerals by infrared laser (1064-nm Nd:YAG laser) was impossible, which was because the strong thermal effect generated by the infrared laser will lead to severe large particle aerosol redeposition. It is reported that ablation systems with shorter wavelengths, such as ultraviolet lasers, including the 266 and 213nm laser, can be used to obtain acceptable analytical accuracy by reducing the thermal effect and aerosol particle size, but a poor precision was still observed<sup>[16-17]</sup>. Guillong et al<sup>[19]</sup> conducted a comparative study of 266, 213 and 193nm lasers and found that there were finer particle sizes of the aerosols and the weaker thermal effect when using 193nm laser ablation, and the RSDs of all elements less than 20% were obtained. In other words, collisions between photons and matter intensify in deep ultraviolet laser ablation systems (193nm) with shorter wavelength<sup>[20-21]</sup> and can help reduce the melt zone and aerosol particle size. However, there is still a slight thermal effect during 193nm UV laser ablation. Fernández et al<sup>[22]</sup> found that there is still a melting layer during 193nm laser ablation, and it leads to the formation of large particle aerosols. Different methods have been proposed to improve the thermal effect during laser ablation of sulfide. Muller et al<sup>[25]</sup> found that the precision of line scanning could be improved by 50% compared to spot ablation. Guillong's results showed that adding a small amount of hydrogen to the analysis could increase the sensitivity of the 47 elements in the test by two to four times<sup>[26]</sup>. Moreover, research has focused on improving the thermal effect of sulfide minerals from shorter pulse width lasers and aerosol particle transport<sup>[27-31]</sup>. However, there are still some thermal effects in the process of deep ultraviolet and short wavelength laser ablation, and how to inhibit the thermal effect in the process of ablation to obtain effective analysis results is still a difficulty in the analysis of sulfide mineral elements. The LA-ICP-MS

low temperature ablation cell is an ablation system developed in recent years, whose main function is to provide a low temperature ablation environment to realize the effective analysis of cells, blood and other samples. The low-temperature ablation cell may be a new approach to resolve the thermal effect during sulfide mineral ablation.

**OBJECTIVES:** In order to establish a high precision and high accuracy multi-element analysis method for sulfide minerals.

**METHODS:** The use of a designed cryogenic ablation cell suppressed the thermal effect and refined aerosol particle sizes, which improved analytical precision and accuracy significantly. To explore the mechanism of sulfide ablation at low temperature, the aerosols ablated at low temperature were collected using an aerosol collection setup consisting of a membrane with an aperture of  $0.1\text{ }\mu\text{m}$ , which was installed at the outlet of the ablation cell. According to the micro-analysis results, the laser ablation behavior under low temperature ablation environment was further discussed.

**RESULTS:** A precision and accuracy method for multi-elements analysis of sulfide minerals using CLA-ICP-MS (laser ablation inductively coupled plasma mass spectrometry with a cryogenic ablation cell) was described. Ablation craters were investigated via scanning electron microscope (SEM) images to compare the amounts of melt produced. SEM measurements showed significant differences in melting between the low temperature ( $-30^{\circ}\text{C}$ ) and room temperature ( $20^{\circ}\text{C}$ ). The diameters and size distribution of particles were measured from nanometer particle potentiometer images of the collected ablated aerosol. Particles ablated using cryogenic ablation cell were smaller in average diameter (190nm and 400nm) and shorter in distribution range (570nm). Compared to the precision of time-resolved signal during laser ablation processes between the two temperatures, the precision was significantly improved and the RSD was reduced from 20.1%-34.4% to 11.5%-15.8% with a cryogenic ablation cell.

A designed cryogenic ablation cell in sulfide sample analysis was utilized to minimize the thermal effect and improve analytical precision and signal intensity. In this study, the CRM (MASS-1) sample was analyzed with spot ablation mode at low ( $-30^{\circ}\text{C}$ ) and room ( $20^{\circ}\text{C}$ ) temperatures, respectively, and the RSDs of three times parallel analysis at these two temperatures were compared. At room temperature, the RSDs of elemental signals ranged from 20.1% to 34.4%. In contrast, the RSD of elemental signals was less than 15.8% when the sample was ablated at low temperature (Fig.2a). The significant improvements may be attributed to low ablation temperature, which suppress the thermal effect. Moreover, the signal intensities of elements improved by approximately 11% to 52% with the decrease in temperature of the cryogenic ablation cell (Fig.2b). Fig.2c shows the time-resolved signals of the MASS-1 sample at room temperature, the significant fluctuations and spikes could be observed, and the RSDs of all elemental signals was more than 20.1%. Interestingly, the signals at low temperature exhibited ideal stability, and the RSDs of elemental signals were less than 15.8%, as shown in Fig.2d.

In order to explore the reasons for improving the analytical performance of low temperature, the morphology of ablation under different temperature conditions of two standard sulfide samples were discussed. SEM images of four ablation craters on chalcopyrite and pyrite were taken to investigate the effect of temperature on the ablation process (Fig.3). The sulfide samples were ablated using a 193nm excimer laser with a spot size of 60nm and a fluence of  $8\text{J}/\text{cm}^2$ . The ablation craters on the chalcopyrite showed a two-layer cyclic structure, in which the inner layer was a light-colored melting zone, and the outer layer was a white aerosol vapor sediment. At low temperature, there were fewer melt layers and thinner grain sediment zone than those at room temperature (Fig.3a, Fig.3b). However, the melting zone around the ablation craters of pyrite were more irregular. More of the unwanted ablation was melted away at room temperature (Fig.3c, Fig.3d). The craters formed at room temperature (Fig.3a, Fig.3c) showed a more

serious melting phenomenon than those formed at low temperature ([Fig.3b](#), [Fig.3d](#)), as evidenced by the abundance of molten ejecta around the former, especially at high laser energy densities. In contrast, the low temperature craters showed no obvious melting phenomenon and had a flatter bottom with a reduced number of large molten spherical particles. The use of CLA-ICP-MS weakened the melting phenomenon, thereby generating smaller aerosol particles, which further improved the aerosol transport and ionization efficiency.

A particle size collection experiment was conducted to explore the distribution of aerosol particles at different temperatures. SEM images were used to analyze the shapes and sizes of particles that were collected on a membrane with an aperture of  $0.1\mu\text{m}$  at room temperature ( $20^\circ\text{C}$ ) and low temperature ( $-30^\circ\text{C}$ ). The same sample chamber and  $1\text{m}$  of tubing were used to transport the particles, and the ablation pulses continuously for  $2\text{min}$ . The SEM images showed that the particles produced at room temperature were larger and formed large agglomerates ([Fig.4a](#)), whereas the particles produced at  $-30^\circ\text{C}$  were smaller and there were fewer agglomerations ([Fig.4c](#)). The shape of the agglomerates and their connection by filaments suggested strong charge during particle formation, which was more prominent at room temperature. Additionally, there were more single large particles produced at room temperature ([Fig.4b](#)), while there were fewer particles at  $-30^\circ\text{C}$  ([Fig.4d](#)). Comparative measurements were conducted using  $193\text{nm}$  laser to investigate the influence of temperatures on particle size distribution. [Fig.4](#) shows a typical size distribution for LA under He atmosphere. The left part of [Fig.5](#) shows a distribution of aerosols produced by ablation of  $2\text{min}$  pulses at room temperature. The peak heights of mean diameter in this distribution were determined to be approximately  $300\text{nm}$  and  $700\text{nm}$ , respectively. Similarly, particle size distribution at  $-30^\circ\text{C}$  also presented a bimodal pattern, which was consistent with previous studies. The average diameters were  $190\text{nm}$  and  $400\text{nm}$ , both smaller than at room temperature, while the peak width was shorter. The chemical composition of fine particles produced at low temperature is closer to the sample body, improving the transport and ionization of aerosol in ICP, reducing element fractionation, and enhancing the signal strength and stability, thereby improving the analytical performance of ICP-MS.

**CONCLUSIONS:** A new high-precision and accuracy method for determination of trace elements in sulfide minerals has been developed using the CLA-ICP-MS system. This method reduces thermal effect and decreases particle size during the ablation process, improving precision by freezing sulfide samples with a designed cryogenic ablation cell. Low temperature results in better data because fewer large particles are produced; sedimentation around the ablation crater and during transport is reduced, while ionization efficiency in ICP is higher. The precision calculated for transient signals decreases obviously if the sample is kept at low temperature ( $-30^\circ\text{C}$ ) compared to room temperature ( $20^\circ\text{C}$ ), while the sensitivity improved slightly. The deviation of all elements between the test values and the standard values falls within 7% by CLA-ICP-MS. In future work, it will be necessary to investigate even lower temperatures, as low temperatures can increase aerosol viscosity and affect analysis results. It is also worth exploring whether the performance of a long pulse width laser can be improved by lowering the temperature to match that of a short pulse width laser.

**KEY WORDS:** low temperature ablation cell; sulfide mineral; laser ablation behavior; thermal effect; LA-ICP-MS

## 参考文献

- [1] Cook N J, Ciobanu C L, Pring A, et al. Trace and minor elements in sphalerite: A LA-ICPMS study[J]. *Geochimica et Cosmochimica Acta*, 2009, 73: 4761–4791.
- [2] Zhao H X, Frimmel H E, Jiang S Y, et al. LA-ICP-MS trace element analysis of pyrite from the Xiaoqinling gold district, China: Implications for ore genesis[J]. *Ore Geology Reviews*, 2011, 43: 142–153.
- [3] Deol S, Deb M, Large R R, et al. LA-ICPMS and EPMA studies of pyrite, arsenopyrite and loellingite from the Bhukia—Jagpura gold prospect, Southern Rajasthan, — 980 —

- India: Implications for ore genesis and gold remobilization[J]. *Chemical Geology*, 2012, 326-327: 72-87.
- [4] 闫巧娟, 魏小燕, 叶美芳, 等. 激光剥蚀电感耦合等离子体质谱-电子探针分析白山堂铜矿中的黄铁矿成分[J]. *岩矿测试*, 2016, 35(6): 658-666.
- Yan Q J, Wei X Y, Ye M F, et al. Determination of composition of pyrite in the Baishantang copper deposit by laser ablation-inductively coupled plasma-mass spectrometry and electron microprobe[J]. *Rock and Mineral Analysis*, 2016, 35(6): 658-666.
- [5] Ma X H, Zeng Q W, Tao S Y, et al. Mineralogical characteristics and *in-situ* sulfur isotopic analysis of gold-bearing sulfides from the Qilishan gold deposit in the Jiaodong Peninsula, China[J]. *Journal of Earth Science*, 2021, 32(1): 116-126.
- [6] Zhou C, Yang Z, Sun H, et al. LA-ICP-MS trace element analysis of sphalerite and pyrite from the Beishan Pb-Zn ore district, South China: Implications for ore genesis[J]. *Ore Geology Reviews*, 2022, 150: 105128.
- [7] 张效瑞, 吴柏林, 雷安贵, 等. 砂岩型铀矿成矿期与非成矿期黄铁矿的微区原位Pb同位素识别特征[J]. *岩矿测试*, 2022, 41(5): 717-732.
- Zhang X R, Wu B L, Lei A G, et al. *In-situ* micro-scale Pb isotope identification characteristics of metallogenic and non-metallogenic pyrites in sandstone-type uranium deposits[J]. *Rock and Mineral Analysis*, 2022, 41(5): 717-732.
- [8] Zhang Y Y, Chu F Y, Li Z G, et al. Gold enrichment in hydrothermal sulfides from the Okinawa Trough: An *in situ* LA-ICP-MS study[J]. *Ore Geology Reviews*, 2020, 116: 103255.
- [9] Yang W W, Zhao H, Zhang W, et al. A simple method for the preparation of homogeneous and stable solid powder standards: Application to sulfide analysis by LA-ICP-MS[J]. *Spectrochimica Acta Part B: Atomic Spectroscopy*, 2021, 178: 106124.
- [10] Qi Y Q, Hu R Z, Gao J F, et al. Trace and minor elements in sulfides from the Lengshuikeng Ag-Pb-Zn deposit, South China: A LA-ICP-MS study[J]. *Ore Geology Reviews*, 2022, 141: 104663.
- [11] Yang Q, Zhang X J, Ulrich T, et al. Trace element compositions of sulfides from Pb-Zn deposits in the Northeast Yunnan and Northwest Guizhou Provinces, SW China: Insights from LA-ICP-MS analyses of sphalerite and pyrite[J]. *Ore Geology Reviews*, 2022, 141: 104639.
- [12] 员媛娇, 范成龙, 吕喜平, 等. 电子探针和LA-ICP-MS技术研究内蒙古浩尧尔忽洞金矿床毒砂矿物学特征[J]. *岩矿测试*, 2022, 41(2): 211-225.
- Yuan Y J, Fan C L, Lyu X P, et al. Application of EPMA and LA-ICP-MS to study mineralogy of arsenopyrite from the Haoyaerhudong gold deposit[J]. *Rock and Mineral Analysis*, 2022, 41(2): 211-225.
- [13] Watling R J, Herbert H K, Abell I D. The application of laser ablation-inductively coupled plasma-mass spectrometry (LA-ICP-MS) to the analysis of selected sulphide minerals[J]. *Chemical Geology*, 1995, 124: 67-81.
- [14] Watling R J. In-line mass transport measurement cell for improving quantification in sulfide mineral analysis using laser ablation inductively coupled plasma mass spectrometry[J]. *Journal of Analytical Atomic Spectrometry*, 1998, 13: 927-934.
- [15] 吴石头, 许春雪, 肖益林, 等. 193nm ArF准分子激光系统对LA-ICP-MS分析中不同基体的剥蚀行为和剥蚀速率探究[J]. *岩矿测试*, 2017, 36(5): 451-459.
- Wu S T, Xu C X, Xiao Y L, et al. Study on ablation behaviors and ablation rates of a 193nm ArF excimer laser system for selected substrates in LA-ICP-MS analysis[J]. *Rock and Mineral Analysis*, 2017, 36(5): 451-459.
- [16] Bacon J R, Crain J S, Vaeck L V, et al. Atomic mass spectrometry[J]. *Journal of Analytical Atomic Spectrometry*, 1999, 14: 1633-1659.
- [17] Günther D, Horn I, Hattendorf B. Recent trends and developments in laser ablation ICP mass spectrometry[J]. *Fresenius Journal of Analytical Chemistry*, 2000, 368: 4-14.
- [18] Hergenröder R. Laser-generated aerosols in laser ablation for inductively coupled plasma spectrometry[J]. *Spectrochimica Acta Part B: Atomic Spectroscopy*, 2006, 61: 284-300.
- [19] Guillong M, Horn I, Günther D. A comparison of 266nm, 213nm and 193nm produced from a single solid state Nd: YAG laser for laser ablation ICP-MS[J]. *Journal of Analytical Atomic Spectrometry*, 2003, 18: 1224-1230.
- [20] Günther D, Heinrich C A. Comparison of the ablation behaviour of 266nm Nd: YAG and 193nm ArF excimer lasers for LA-ICP-MS analysis[J]. *Journal of Analytical Atomic Spectrometry*, 1999, 14: 1369-1374.
- [21] Liu Y S, Hu Z C, Li M, et al. Applications of LA-ICP-MS in the elemental analyses of geological samples[J]. *Chinese Science Bulletin*, 2013, 58: 3863-3878.
- [22] Fernández B, Claverie F, Péchéyran C, et al. Direct analysis of solid samples by fs-LA-ICP-MS[J]. *Trends*

- in *Analytical Chemistry*, 2007, 26: 951–966.
- [23] 柯于球, 张路远, 柴辛娜, 等. 硫化物矿物 LA-ICP-MS 激光剥蚀元素信号响应[J]. *高等学校化学学报*, 2012, 33(2): 257–262.
- Ke Y Q, Zhang L Y, Chai X N, et al. Elemental signal response of sulfide minerals in LA-ICP-MS microanalysis[J]. *Chemical Journal of Chinese Universities*, 2012, 33(2): 257–262.
- [24] Kuhn H R, Günther D. Laser ablation-ICP-MS: Particle size dependent elemental composition studies on fifilter-collected and online measured aerosols from glass[J]. *Journal of Analytical Atomic Spectrometry*, 2004, 19: 1158–1164.
- [25] Mueller W, Shelley J, Rasmussen S. Direct chemical analysis of frozen ice cores by UV-laser ablation ICPMS[J]. *Journal of Analytical Atomic Spectrometry*, 2011, 26: 2391–2395.
- [26] Guillong M, Heinrich C A. Sensitivity enhancement in laser ablation ICP-MS using small amounts of hydrogen in the carrier gas[J]. *Journal of Analytical Atomic Spectrometry*, 2007, 22: 1488–1494.
- [27] Bogaerts A, Chen Z, Gijbels R, et al. Laser ablation for analytical sampling: What can we learn from modeling[J]. *Spectrochimica Acta Part B: Atomic Spectroscopy*, 2003, 58: 1867–1893.
- [28] Poitrasson F, Mao X L, Mao S S, et al. Comparison of ultraviolet femtosecond and nanosecond laser ablation inductively coupled plasma mass spectrometry analysis in glass, monazite, and zircon[J]. *Analytical Chemistry*, 2003, 75: 6184–6190.
- [29] Liu C, Mao X L, Mao S S, et al. Nanosecond and femtosecond laser ablation of brass: Particulate and ICPMS measurements[J]. *Analytical Chemistry*, 2004, 76: 379–383.
- [30] Telouk P, Rose-Koga E F, Albareda F. Preliminary results from a new 157nm laser ablation ICP-MS instrument: New opportunities in the analysis of solid samples[J]. *Geostandards and Geoanalytical Research*, 2003, 27: 5–11.
- [31] Wohlgemuth-Ueberwasser C C, Jochum K P. Capability of fs-LA-ICP-MS for sulfide analysis in comparison to ns-LA-ICP-MS: Reduction of laser induced matrix effects[J]. *Journal of Analytical Atomic Spectrometry*, 2015, 30: 2469–2480.
- [32] Reinhardt H, Kriewa M, Miller H, et al. Laser ablation inductively coupled plasma mass spectrometry: A new tool for trace element analysis in ice cores[J]. *Fresenius Journal of Analytical Chemistry*, 2001, 370(5): 629–636.
- [33] Feldmann J, Kindness A, Ek P. Laser ablation of soft tissue using a cryogenically cooled ablation cell[J]. *Journal of Analytical Atomic Spectrometry*, 2002, 17(8): 813–818.
- [34] Wang Y, Wei X, Liu J H, et al. Cryogenic laser ablation in a rapid cooling chamber ensures excellent elemental imaging in fresh biological tissues[J]. *Analytical Chemistry*, 2022, 94(23): 8547–8553.
- [35] Li F, Lei X Q, Li H L, et al. Direct multi-elemental analysis of whole blood samples by LA-ICP-MS employing a cryogenic ablation cell[J]. *Journal of Analytical Atomic Spectrometry*, 2023, 38: 90–96.
- [36] Li F, Cui H, Zhang D W, et al. Direct multi-elemental analysis of cerebrospinal fluid samples by LA-ICP-MS employing an aerosol local extraction cryogenic ablation cell[J]. *Journal of Analytical and Bioanalytical Chemistry*, 2023, 415: 6051–6061.
- [37] Wilson S A, Ridley W I, Koenig A E. Development of sulfide calibration standards for the laser ablation inductively-coupled plasma mass spectrometry technique[J]. *Journal of Analytical Atomic Spectrometry*, 2002, 17: 406–409.
- [38] Jarošová M, Walaszek D, Wagner B, et al. Influence of temperature on laser ablation fractionation during ICP-MS analysis for 213nm and 266nm laser wavelength micro-sampling[J]. *Journal of Analytical Atomic Spectrometry*, 2016, 31: 2089–2093.
- [39] Koch J, von Bohlen A, Hergenröder R, et al. Particle size distributions and compositions of aerosols produced by near-IR femto- and nanosecond laser ablation of brass[J]. *Journal of Analytical Atomic Spectrometry*, 2004, 19: 267–272.
- [40] Li Z, Hu Z C, Günther D, et al. Ablation characteristic of ilmenite using UV nanosecond and femtosecond lasers: Implications for non-matrix-matched quantification[J]. *Geostand Geoanalytical Research*, 2016, 40: 477–491.
- [41] Longerich H P, Günther D, Jackson S E. Elemental fractionation in laser ablation inductively coupled plasma mass spectrometry[J]. *Fresenius Journal of Analytical Chemistry*, 1996, 355: 538–542.